# Use of pyrite microfabric as a key to tectono-thermal evolution of massive sulphide deposits — an example from Deri, southern Rajasthan, India

Anju Tiwary, Mihir Deb

Department of Geology, Delhi University, Delhi 10007, India

AND

Nigel J. Cook

Mineralogical Institute, University of Würzburg, Am Hubland, D-97074 Würzburg, Germany

## ABSTRACT

Pyrite is an ubiquitous constituent of the Proterozoic massive sulphide deposit at Deri, in the South Delhi Fold Belt of southern Rajasthan. Preserved pyrite microfabrics in the Zn-Pb-Cu sulphide ores of Deri reveal a polyphase growth history of the iron sulphide and enable the tectono-thermal evolution of the deposit to be reconstructed.

Primary sedimentary features in Deri pyrites are preserved as compositional banding. Regional metamorphism from mid-greenschist to low amphibolite facies is recorded by various microtextures of pyrite. Trails of fine grained pyrite inclusions within hornblende porphyroblasts define $S_1$-schistosity. Pyrite boudins aligned parallel to $S_1$ mark the brittle–ductile transformation of pyrite during the earliest deformation in the region. Isoclinal to tight folds ($F_1$ and $F_2$) in pyrite layers relate to a ductile deformation stage during progressive regional metamorphism. Peak metamorphic conditions around 550°C, an estimation supported by garnet–biotite thermometry, resulted in annealing of pyrite grains, while porphyroblastic growth of pyrite (up to 900 µm) took place along the retrogressive path. Brittle deformation of pyrite and growth of irregular pyritic mass around such fractured porphyroblasts characterize the waning phase of regional metamorphism. A subsequent phase of stress-free, thermal metamorphism is recorded in the decussate and rosette textures of arsenopyrite prisms replacing irregular pyritic mass. Annealing of such patchy pyrite provides information regarding the temperature conditions during this episode of thermal metamorphism which is consistent with the hornblende-hornfels facies metamorphism interpreted from magnetite–ilmenite geothermometry (550°C) and sphalerite geobarometry (3.5 kbar). A mild cataclastic deformation during the penultimate phase produced microfaults in twinned arsenopyrite prisms.

KEYWORDS: pyrite, microfabric, metamorphism, massive sulphide, Rajasthan, India.

## Introduction

METAMORPHOSED pyrite has been shown to exhibit mainly cataclastic fabrics and behaves in a brittle fashion over a wide range of geological conditions (Graf and Skinner, 1970), particularly below ~ 450°C (Cox *et al.*, 1981). It has, however, been experimentally demonstrated that pyrite may also yield by dislocation processes at higher temperatures, between 400–700°C (Cox *et al.*, 1981; Graf

*et al.*, 1981). Ductile deformation, although only reported for naturally deformed pyrites in a few instances (e.g. Mookherjee 1971; Sarkar and Deb, 1974; Cook *et al.*, 1993), has been experimentally found to take place at conditions higher than 450°C at 300 MPa (Cox *et al.*, 1981). McClay and Ellis (1984) however, demonstrated that pressure solution, that is, fluid-assisted mass transfer, and cataclastic flow are the dominant deformation mechanisms in pyrite in a low-grade metamorphic

environment. These authors (1983) also point out that at higher metamorphic conditions, post-tectonic annealing and grain growth would tend to erase most of the earlier deformation features.

Pyrite is the predominant mineral formed or modified during a broad spectrum of ore-forming processes. Regional metamorphism commonly obliterates primary textures, but recent studies have shown that the refractory nature of pyrite does allow it to preserve features both of pre-metamorphic origin and also those formed in the early stages of metamorphism (cf. Craig and Vokes, 1993). Therefore an understanding of the retention of pre-, syn- and post-metamorphic features in pyrite can have wide ranging potential in deciphering the evolutionary history of a metamorphosed orebody. Pyrite, an ubiquitous constituent of the Deri massive sulphide deposit in southern Rajasthan, India, displays primary depositional features as well as common brittle and rare ductile deformation fabrics, along with porphyroblastic growth, recrystallization and annealing textures. This paper examines such pyrite microfabrics and aims to use these growth features and relationships with co-existing silicates to trace the tectonothermal history of the deposit. The approach followed here has been commonly applied to porphyroblastic silicate minerals such as garnet, cordierite, andalusite etc. by metamorphic petrologists (e.g. Vernon, 1978).

## Geological setting

The South Delhi fold belt (SDFB) constitutes the western fringe of the Proterozoic Aravalli-Delhi orogenic belt in NW India (Deb and Sarkar, 1990). This belt hosts a number of VMS-type deposits and prospects located close to its western margin, which show Pb-Pb model ages between 1100 and 990 Ma (Deb et al., 1989; Deb et al., under prep.). The massive sulphide deposit at Deri is located in the southern most part of SDFB (Fig. 1) and has an estimated reserve of approximately 1 million metric tonnes, grading 9% Zn,
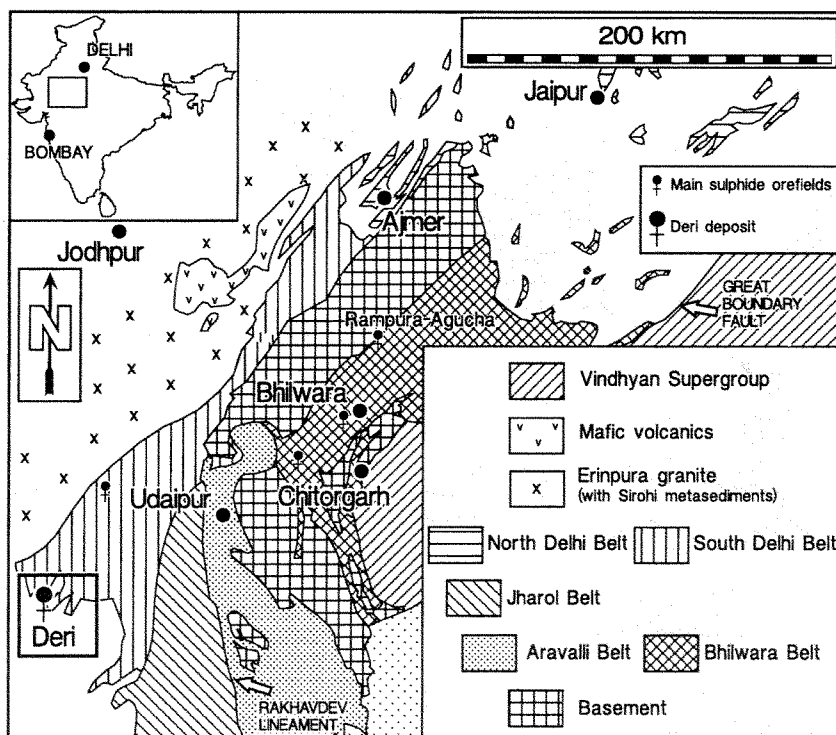


FIG. 1. Geological map of the Aravalli-Delhi orogenic belt (modified after Deb and Sarkar, 1990).

6.8% Pb, and 1.1% Cu (Deb, 1980). The volcano-sedimentary package underlying this deposit constitutes the upper part of the Ajabgarh Group of the Delhi Supergroup ( Heron, 1953; Roy, 1988). It comprises a bimodal volcanic suite (Bhattacharjee *et al.*, 1988) of mafic meta-tholeiites (amphibolites) and felsic meta-rhyolites (chloritic hornfels) with minor amounts of meta-andesites. The interlayered sediments are repre-sented by biotite-quartz schist, paragneiss and biotite gneiss. The volcano-sedimentary package has been subsequently intruded by alkali syenite bodies (Fig. 2) (Tiwary, 1995). This plutonic activity is thought to be contemporaneous with the phase of felsic plutonism in the SDFB which occurred between 850 to 750 Ma (Gopalan, 1986).

The Deri deposit is composed of stratiform massive, banded and disseminmated sulphides defining four sulphide lenses, occurring within a restricted ($\sim 200$ m) stratigraphic interval. The
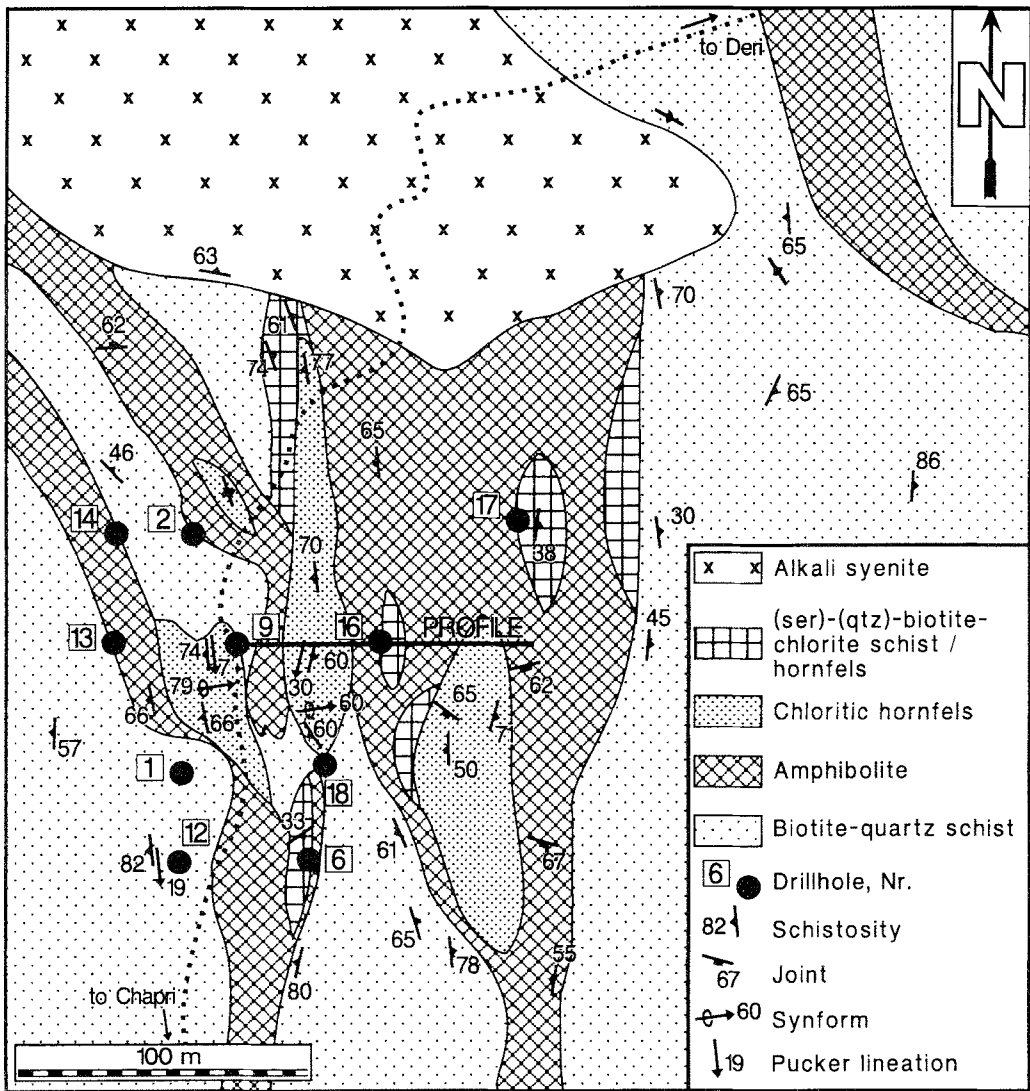


FIG. 2. Simplified geological map of Deri ore zone (modified from Deb, 1980).

lenses are peneconcordant with sub-vertical dipping schistosity surfaces and litho-contacts in the altered bimodal volcanics. The host rocks enclosing the deposit are represented by three distinct semi-conformable alteration facies (Fig. 3), all characterized by conspicuously magnesian mineralogy: hornblende-biotite-plagioclase-quartz schist (AMMV), cordierite-anthophyllite-chlorite hornfels (AFMV) and (seri-cite)-biotite-chlorite schist/hornfels (BCS) (Tiwary and Deb, 1997). Tourmaline-rich meta-chert (MC) in the ore zone represents a metamorphosed exhalite horizon. Detailed geological, petrological and geochemical investiga-

tions, including a consideration of Pb, S and B isotopic signatures enabled Tiwary (1995) to propose a genetic model for this deposit involving pre-metamorphic, exhalative seafloor deposition (VMS-type).

In the Deri underground mine, three generations of folds can be recognized on a mesoscopic scale. Pyrite layers in AFMV show hook-shaped isoclinal folds which are considered to belong to the earliest generation of $(F_1)$ folds in the region. These folded layers involve primary stratification $(S_0)$ in the host rocks and have developed axial plane foliation $(S_1)$. Tight, upright to inclined, shallow plunging folds on both $S_0$ and $S_1$ in the
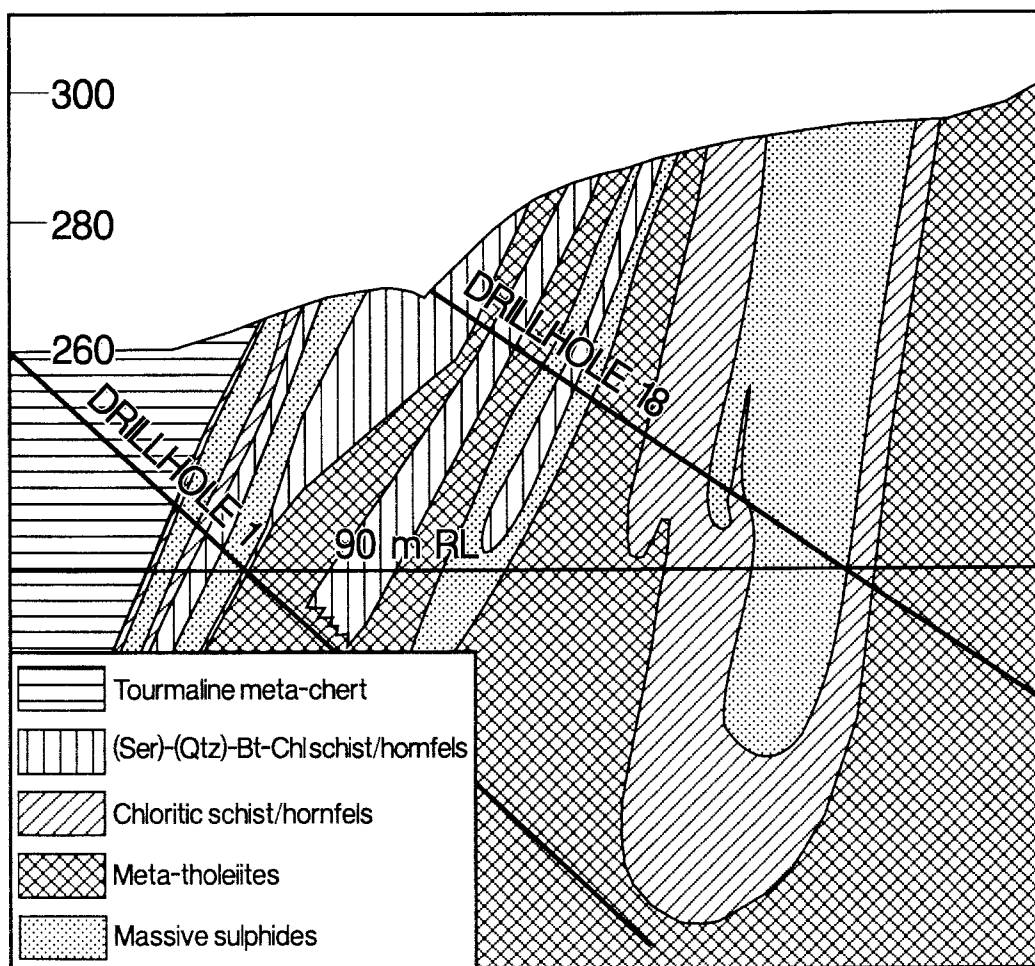


FIG. 3. E—W transverse section across the Deri deposit between drill holes 1 and 18 (after Tiwary, 1995).

ore-host rocks represent a subsequent generation of $F_2$-folds. Both $F_1$ and $F_2$-folds trend N—S and the pervasive axial plane schistosity ($S_2$) of $F_2$-folds is sub-parallel to $S_1$. $S_2$ is indistinguishable from $S_1$ except near the hinge of the $F_2$-folds. A further set of open folds have been noted in the AFMV and in sphalerite-rich banded ores. Their axial traces trend E—W to N75°W—S75°E and dip at low angles towards the south. This generation of folds has affected the pervasive schistosity ($S_2$) as well as the primary stratification ($S_0$). They are, therefore, ascribed to a third episode of folding ($F_3$), when a transposition schistosity ($S_3$) developed incipiently at high angles to $S_2$. A conspicuous dextral fault of limited extent, sub-parallel to the trend of the axial trace of $F_3$-folds, has affected two of the orebodies.

The conditions under which the ore and host rocks at Deri underwent isofacial metamorphism during two distinct phases have been defined by Tiwary (1995). Regional metamorphism took place during the culmination of $F_2$-deformation under low pressure amphibolite facies conditions. The subsequent thermal metamorphism under hornblende-hornfels facies was apparently related to the intrusion of Neo-proterozoic syenite plutons in the area.

## Ore mineralogy and fabric

Ore petrographic observations recorded in this paper were made on diamond drill cores and representative samples collected in the Deri mine at the −80 and −90m levels. Mineralogically, the Deri ores can be classified under four distinct sulphide assemblages:

(1) Sphalerite-rich ores (sl + gn + cp + py + mt)
(2) Galena-rich ores (gn + py + sl + po + asp + thd + bi + bmt+ mb)
(3) Chalcopyrite-rich ores ( cp + po + sl + mt + py + cb +bmt ± mck)
(4) Pyrite-rich ores (py + mt + sl + gn + cp + bi) where bi = native bismuth, bmt = bismuthinite, mck = mackinawite, cb = cubanite, thd = tetrahedrite, mb = molybdenite.

The most common sphalerite-rich ores comprise medium to coarse, polygonal sphalerite grains, often with parallel sided coherent twins (Fig. 4a). They are associated with varying concentrations of pyrite, galena and chalcopyrite. Pyrrhotite and magnetite are also found sporadically. Rarely, flakes of molybdenite within the sphalerite mass and prisms of arsenopyrite,

replacing polycrystalline pyrite aggregates, are also noted. Bright white specks with high reflectivity, identified as bismuthinite, occur in trace amounts in the galena matrix. Galena and chalcopyrite in this association commonly display bleb-like, cuspate and/or stringy habit according to the dihedral angle requirements amongst the phases.

Ores in which galena is predominant, contain medium to coarse pyrite porphyroblasts and subrounded grains of sphalerite in the galena mass. These ores exhibit a varied mineralogy. Fine to medium anhedral grains of tetrahedrite, the most common sulphosalt, occur along the galena—sphalerite interface. Small inclusions of the mineral are also noted within the galena mass. Bismuthinite and native bismuth, intimately intergrown with each other, occur as fine inclusions in the galena matrix. Small flakes of molybdenite are found included within coarse sphalerite aggregates in these ores.

In chalcopyrite-rich ores, pyrrhotite occurs in abundance, more commonly as irregular to subrounded grains, intimately associated with sphalerite, magnetite and pyrite. The presence of minor phases like molybdenite, threads of mackinawite and deformed blades of cubanite are occasionally noted. Rutile and bismuthinite are rare. Excellent development of arsenopyrite on irregular masses of pyrite is observed in some of the chalcopyrite-rich sections.

Pyrite-dominated ores exhibit well developed banding in places, comprising medium to coarse idiomorphic pyrite aggregates interlayered with minor sphalerite, magnetite and galena. Minor phases such as bismuthinite are also observed in the galena matrix.

The sulphides in all assemblages show intimate intergrowth with the associated silicates. Euhedral, coarse amphiboles occur extensively with annealed pyrite aggregates and are also found to trace a well-defined schistosity in the chalcopyrite-pyrrhotite-magnetite mass (Fig. 4b). Where galena is the predominant sulphide, a typical hornfelsic mass of chlorite and amphiboles is often present, or galena is found interlayered with kinked flakes of chlorite (Fig. 4c). Polygonal sphalerite and chalcopyrite aggregates are found intergrown with hornblende prisms displaying a hornfelsic texture (Fig. 4d). Thus the massive sulphide ores of Deri display a variety of well developed metamorphic fabrics (Deb, 1979) while retaining vestigially some primary features, such as compositional layering.
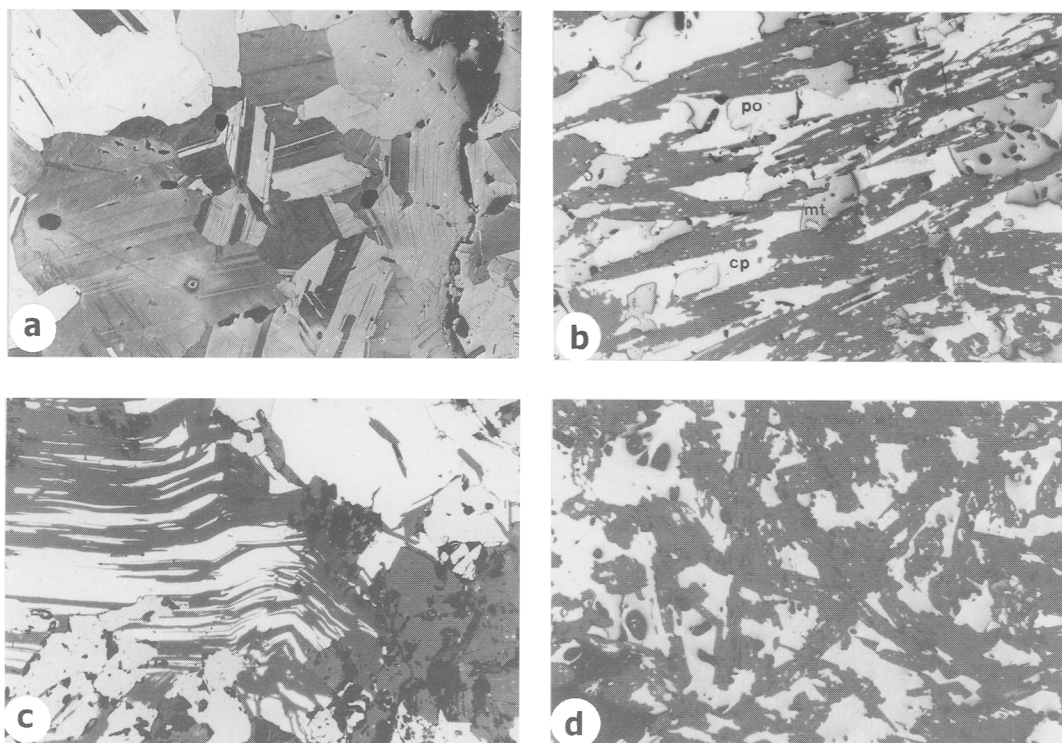
FIG. 4. Photomicrographs of metamorphic fabrics of sulphide ores in reflected light. (*a*) Medium to coarse polygonal sphalerite grains showing coherent annealing twins. Etched with HBr solution. Width of field = 3 mm. (*b*) Coarse amphibole blades tracing well defined schistosity in chalcopyrite (cp), pyrrhotite (po), magnetite (mt) mass. Width of field = 3.04 mm. (*c*) Kinked flakes of chlorite showing interlayering with galena mass. Width of field = 0.94 mm. (*d*) Aggregates of sphalerite and chalcopyrite intergrown with hornblende grains displaying hornfelsic fabric. Width of field = 3.04 mm.

## Pyrite microfabric

Vokes (1968), Templeman-Kluit (1970) and McClay and Ellis (1983) noted a crude correlation between pyrite grain size and metamorphic grade. McClay and Ellis (1983) also recorded a number of other factors including primary/depositional and post-depositional/metamorphic effects, as well as the nature of the matrix, nature of the grain boundaries and pyrite chemistry, which affect pyrite grain size. In the Deri ores, pyrite exhibits both brittle and ductile deformation textures as well as post-deformational annealing, all of which influence pyrite grain size to varying degrees. Rigorous textural and grain size analysis of pyrite using etched sections is therefore essential for an understanding of the metamorphic evolution of these ores. Pyrite-rich polished sections were studied systematically and were also etched with 20% $HNO_3$ to expose otherwise obscured textures. Pyrite microfabrics are described below under six categories: primary; ductile; annealing; recrystallization and growth; brittle and replacement textures, and their textural implications are discussed in a later section.

### Primary textures

Alternating, compositionally distinct bands, rich in pyrite, sphalerite (Fig. 5*a*), galena, magnetite and/or silicates are interpreted as primary depositional features of the ores.

### Ductile deformation textures

In highly deformed Deri ores, fine to medium, elongated pyrite aggregates resemble boudins which have been stretched along the plane of $S_1$-
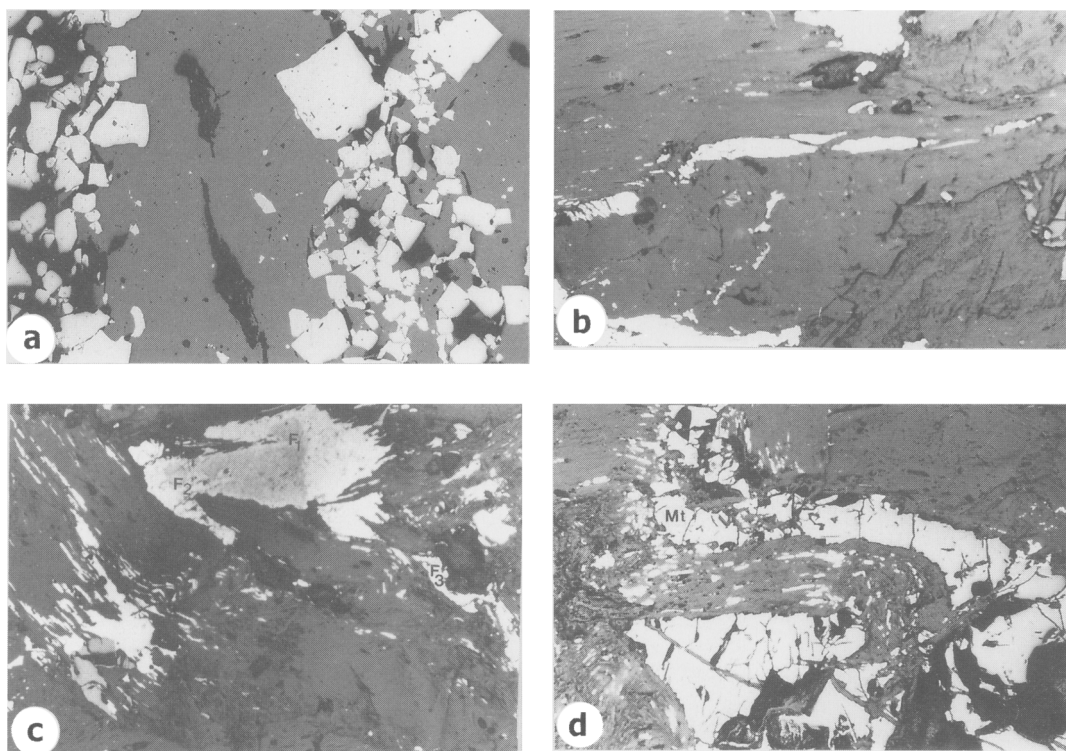
FIG. 5. Photomicrographs of pyrite microfabrics in reflected light. (*a*) Primary banding shown by alternating compositional layers of pyrite and sphalerite. Width of field = 3.25 mm. (*b*) A jigsaw-fit fabric of three pyrite grains (centre of photo) during boudinage of a pyrite grain parallel to $S_1$-foliation of chlorite (see text for discussion). Width of field = 1.52 mm. (*c*) Hook shaped folded pyrite layer, now constituted partly by polycrystalline grains. The axial plane of the isoclinal closures ($F_1$) parallels the $S_1$-schistosity of chlorite fibres while the tight closure ($F_2$) is oriented along the transposed schistosity $S_2$. The thin sheet of pyrite shows open folds ($F_3$), at large angles to the $S_2$-schistosity (see Fig.8 for more details). Width of field = 1.52 mm. (*d*) Participation of magnetite (Mt) in the episode of tight folding defined here by coarse chlorite flakes. Axial plane of the fold is parallel to $S_2$-schistosity. Width of field = 1.52 mm.

schistosity (Fig. 5*b*). Such sections also show deformation of pyrite in the form of isoclinal to tight folding (Fig. 5*c*). The axial plane of the isoclinal closure in the pyrite layer parallels the $S_1$-schistosity. The tight closure on the other end of this folded pyrite (Fig. 5*c*) has its axial trace parallel to the transposed $S_2$-schistosity, defined by crenulated pyrite-chlacopyrite interlayering with chlorite. The axial traces of these crenulations are at high angles to the $S_2$-foliation. Interestingly, a refractory mineral like magnetite, normally considered to deform in a brittle fashion, is also found to be affected by tight folding. The axial planes of such folds are parallel to the pervasive $S_2$-

schistosity which is defined by coarse silicate flakes and interlayered galena streaks (Fig. 5*d*).

### Annealing textures

Compositional layering ($S_0$), mentioned above, is constituted by *in situ* annealed pyrite grains. Pyrite elsewhere, with an average grain size of 400 µm, also forms a mosaic with individual grains meeting with equal interfacial angles at triple junction points. Such grains are commonly found in bands which show alignment parallel to the $S_2$-foliation defined by coarse hornblende porphyroblasts (Fig. 6*a*). Annealing is also observed in the irregular pyritic mass enveloping
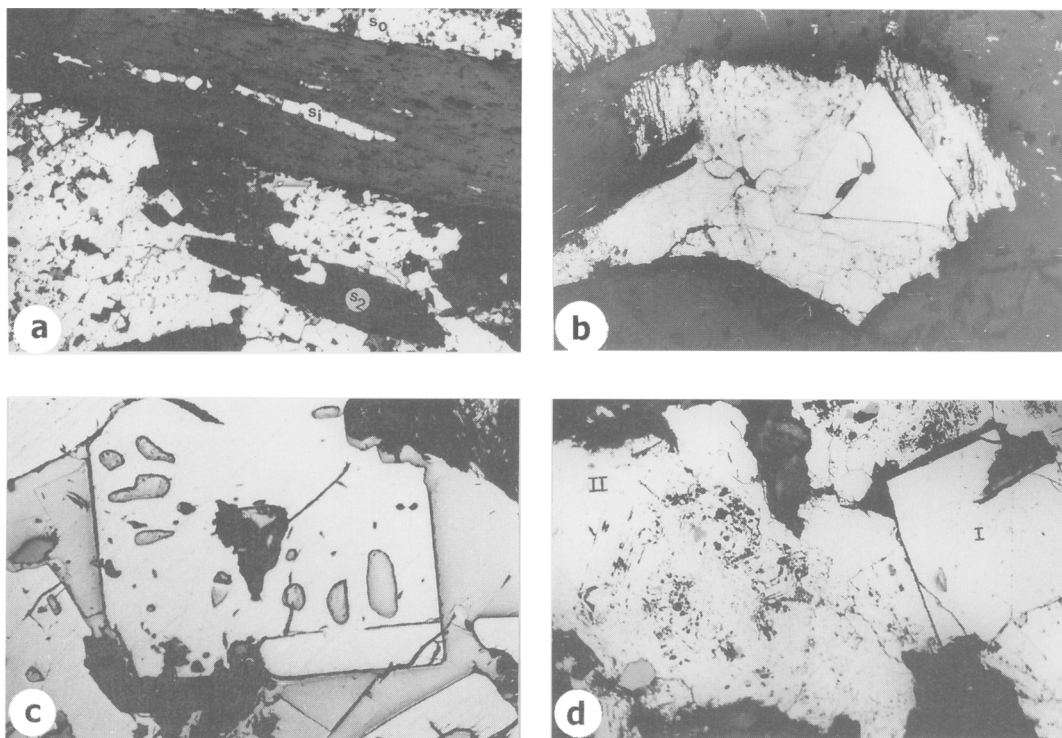
FIG. 6. Photomicrographs of pyrite microfabrics in reflected light. (a) Fine, subhedral pyrite grains, aligned in a plane, defining $S_i = S_1$, enclosed within a coarse amphibole blade. Pyrite outside the blade shows annealed fabric and is aligned in bands ($S_o$) parallel to the schistosity of amphiboles ($S_2$). Width of field = 3.04 mm. (b) Annealed mass of pyrite enclosing idiomorphic, cracked, pyrite porphyroblast. Width of field = 0.76 mm. (c) Euhedral porphyroblast of pyrite with elliptical, radially disposed, inclusions of the galena. The centre of the grain contains an inclusion of a tightly folded chlorite flake. Width of field = 3.04 mm. (d) Idiomorphic, fractured pyrite porphyroblast (I) enclosed within patchy mass of pyrite (II) which displays well developed zonal structure upon etching. Width of field = 1.81 mm.

idiomorphic pyrite porphyroblasts, although here, the grain size is relatively smaller, between 250 to 300 μm (Fig. 6b).

### Recrystallization and growth textures

Fine and idiomorphic pyrite grains (100–150 μm) are found included and aligned along the cleavage of large hornblende porphyroblasts. Merging of such grains produces an apparantly streaked out layer of pyrite inclusions in the host silicate (Fig. 6a). Pyrite porphyroblasts, up to 900 μm, commonly occur in the softer sulphide matrix and display variable degrees of deformation. Most of them, however, retain their idiomorphic shape (Fig. 6c) and also include fine to medium blebs of the matrix sulphides, mostly galena and spha-

lerite. The radial disposition of the inclusions may suggest zoned growth of the idiomorphic poikiloblasts. These larger pyrite grains are also found to include tightly $F_2$-folded phyllosilicates (Fig. 6c), which provide important constraints on the timing of growth and coarsening of pyrite in these ores. Irregular pyrite mass commonly surrounds smaller idiomorphic pyrite porphyroblasts, often characterized by axial cracks. Such pyritic mass locally displays a zonal growth pattern (Fig. 6d) or polygonal fabric (Fig. 6b).

### Brittle deformation textures

Evidence of cataclastic deformation is well preserved in pyrite porphyroblasts which show fracturing, ranging from hairline cracks to

extensive pulverization (Fig. 7a). These intragranular cracks are filled up by softer sulphides like chalcopyrite, galena and sphalerite. Relatively smaller pyrite porphyroblasts, surrounded by irregular pyritic patches, have also undergone brittle deformation as mentioned above.

### Replacement textures

Euhedral pyrite grains show corrosion textures and replacement by softer sulphides like sphalerite and galena. In extreme cases of pyrite replacement, only relicts of these porphyroblasts remain within the enclosing mass of softer sulphides. In other polished sections, arsenopyrite has extensively replaced pyrite aggregates, enclosing relatively smaller pyrite porphyroblasts. Such grains of arsenopyrite are commonly twinned and display a rosette texture indicative of growth under stress-free conditions (Fig. 7b).

### Dircuppion

Four classes of sulphide assemblages are recognized in the Deri deposit. Preserved textures, particularly the pyrite microfabrics, represent evidence for brittle and ductile deformation and post-deformational recrystallization and growth. We now attempt here to relate the pyrite microfabrics described above to the sequence of syngenesis, polyphase deformation and metamorphism established for the area on the basis of mesoscopic structures and petrographic study of crystallization-deformation and sulphide-silicate relationships (Tiwary, 1995).

A primary syn-diagenetic volcano-sedimentary feature is preserved in the form of compositional banding in the ores, defined by alternate layers of pyrite, magnetite, sphalerite, and/or silicates, all of which have recrystallized *in situ* (Fig. 5a).

At the initiation of the regional metamorphic event, during the first phase of deformation, primary banding of pyrite with silicates underwent isoclinal folding. These first generation of folds are best preserved on a mesoscopic scale (as mentioned in an earlier section) and are rarely seen in polished sections. However, a fine schistosity is well preserved as inclusion trails of pyrite in silicate porphyroblasts of cordierite, andalusite and hornblende, which themselves define the $S_2$-foliation (Tiwary, 1995). The fine grain-size (150 μm) and straight orientation of the inclusions (Fig. 6a) warrant their recognition as $S_1$-foliation formed during the earliest deformation episode (cf. Vernon *et al.*, 1991). Such fine-grained idiomorphic development of pyrite grains at the expense of original sedimentary-diagenetic pyrite granules possibly took place due to the constraints exerted by the cleavage planes of the bladed host silicates. We may therefore infer that this class of pyrite in the Deri ores grew during the initial prograde path of regional metamorphism, coinciding with the first deformation.

Subsequent progressive deformation involved $S_1$-schistosity and produced a second generation of tight, generally co-axial, folds whose axial plane schistosity defines a distinct $S_2$-foliation. An interesting evidence of transposition of $S_1$ into $S_2$ schistosity is seen in the microstructural
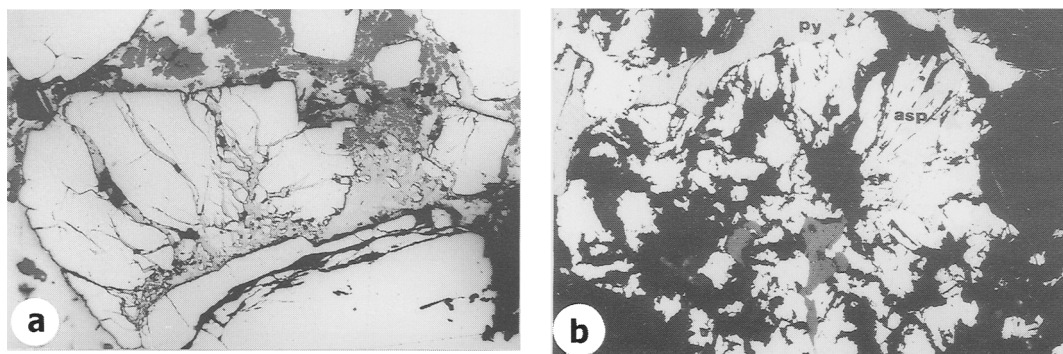
FIG. 7. Photomicrographs of pyrite microfabrics in reflected light. (a) Brittle deformation of pyrite in which fractures have channelled more ductile sulphides, chiefly chalcopyrite with some sphalerite, which have replaced and corroded the porphyroblasts. Width of field = 3.25 mm. (b) Radial growth of arsenopyrite prisms (asp) over irregular mass of pyrite (py) (half crossed nicols). Width of field = 2.71 mm.

relationships (Fig. 8) noted in one polished section. The $S_1$ schistosity here encloses boudinaged pyrite fragments and is also axial planer to an isoclinally folded hook-shaped pyrite layer. The transposed $S_2$-schistosity transects $S_1$ at 45° producing marked alignment of coarse phyllosilicates. The zone of transposition has affected the folded pyrite layer at the upper end (Fig. 8) producing a tight fold whose axial plane shows parallelism to $S_2$-schistosity. This fold closure is therefore ascribed to the $F_2$ deformation. It may not be out of place here to reflect on the various mechanisms through which boudinaged and folded pyrite fabric could develop:

1. Post-tectonic replacement of deformed silicates, e.g. hornblende, by pyrite.
2. Polycrystalline pyrite aggregates subjected to brittle–ductile deformation and stretched or folded into their present shape.
3. Individual pyrite grains involved in progressive shear and ductile stretching during $F_1$ folding

resulting in the development of isoclinal folds and/or boudins.

In the first case, such perfect and selective replacement would be extremely fortuitous. Secondly, when a polycrystalline aggregate is stretched, the weakness along the grain boundaries would result in separation of the grains at the point of maximum stress. It should thus be impossible, even assuming another subsequent recrystallization during thermal metamorphism, to produce the type of perfect jigsaw-fit seen in the pyrite boudin (Fig. 5b). We thus prefer the third alternative, in which a pyrite grain undergoes deformation in the field of brittle–ductile transition and continues to be deformed in the ductile field. The folded pyrite is parallel to the $S_1$-foliation and has presumably undergone simple shear during flexture-slip $F_1$-folding. In detail, development of the pyrite boudins may be considered in terms of progressive simple shear (cf. Ghosh, 1993) (Fig. 9a−c). In such deforma-
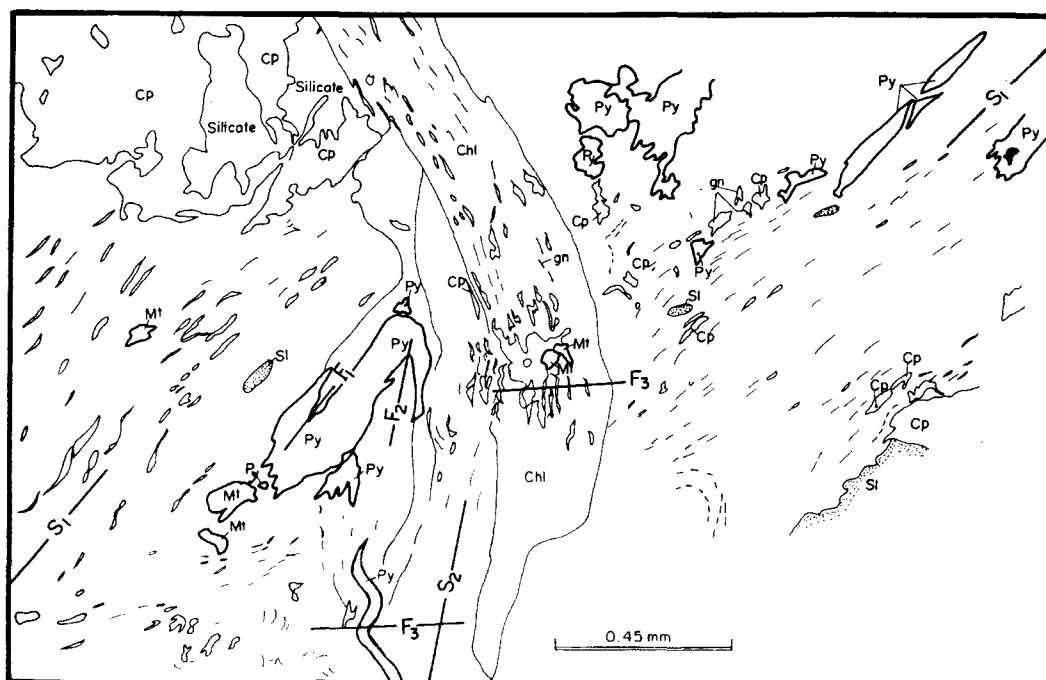


FIG. 8. Camera-lucida sketch showing microstructural relationships of the folded and boudinaged pyrite (Py) (shown in Fig. 5c and b respectively). $S_1$-schistosity of chlorite is axial planer to isoclinally folded ($F_1$) hook-shaped pyrite layer and is also sub-parallel to boudinaged pyrite. $S_2$-schistosity transects $S_1$-foliation at 45° and has affected the folded pyrite layer at the upper end ($F_2$) producing tight fold whose axial plane is parallel to $S_2$. The warp of the coarse chlorite (chl) flake and the open folds ($F_3$) of pyrite have their axial planes at high angle to $S_2$.
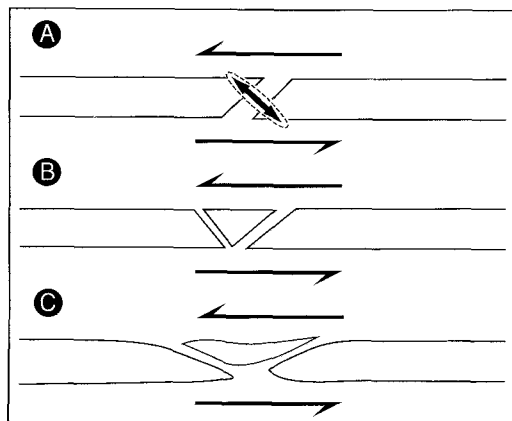
FIG. 9. Conjectured mechanism of boudin development seen in Fig. 5b: (a) Formation of gash at 90° to principal strain axes, (b) Brittle rupture along principal extension direction of the strain ellipse, (c) Ductile extension of pyrite boundins with chlorite infilling the fracture (see text for discussion).

tion, a circle is transformed into an ellipse with the principal axes of the strain ellipsoid changing position with progressive simple shear. Tension gashes develop at approximately 90° to the principal extension direction of the strain ellipsoid and at about 45° to the shear plane (Sugden, 1987). Hence, the fabric may have developed by: (i) formation of a gash at 45° to the shear direction (Fig. 9a), followed by (ii) brittle rupture of one of the pyrite fragments along the principal extension direction (Fig. 9b) due to rheological contrast between pyrite and the less competent chloritic matrix, and finally (iii) ductile extension of the pyrite boudins occurred with the chlorite infilling the fractures (Fig. 9c). Since a brittle–ductile transition is perceived for this microfabric, the temperature conditions may be deduced to be just above 400°C (Cox et al., 1981) during the development of $S_1$ along which these boudins are aligned.

The isoclinal fold in the pyrite layer enclosed within the $S_1$ foliation (Figs. 5c and 8) may also be interpreted by the parallel layer shear mechanisms discussed above. Small buckles are initiated due to continuous fluctuations in the rate of shear, along the $S_1$ schistosity. Continued shear led to passive amplification and tightening of such fold closures (Fig. 8).

Involvement of the $F_1$-folded pyrite layer in the transposition of the $S_1$-schistosity, producing the

tight fold parallel to $S_2$-foliation, suggests continued ductile behavior of pyrite during the phase of $F_2$-deformation. A polygonal mosaic of pyrite in bands parallel to the hornblende schistosity ($S_2$), but without any preferred orientation, suggests post-$F_2$ annealing of pyrite (Fig. 6a). Such a fabric also provide useful information regarding the prevailing metamorphic conditions. According to Cox et al. (1981), dynamic recovery and recrystallization are important processes of pyrite growth above 550°C. In the light of these experimental data, ductile behavior of pyrite may be envisaged to have occurred at around 450°C, followed by recrystallization with increasing temperature to produce annealed polycrystalline pyrite around 550°C, defining the post-$F_2$ peak of regional metamorphism. The presence of hornblende blades in the ores indicates attainment of amphibolite facies conditions during development of $S_2$ planes. Hence the $P-T$ conditions during the peak of regional metamorphism must have reached a minimum of 550°C at a pressure of 4 kbar (Philpotts, 1994), an estimate consistent with the requirement for granoblastic pyrite growth. Regional metamorphic conditions during the second deformation at Deri were also derived directly from the compositions of co-existing garnet and biotite oriented parallel to $S_2$-foliation, indicating syn-$F_2$ growth. The garnets display no zonation, suggesting single stage growth in equilibrium with co-existing biotite. Temperatures in the range 500–560°C were obtained, using a range of calibrations (Table 1). The high (ca. 30%) spessartine component does, however, cause difficulties in geothermometric estimations of the Deri assemblage, and the estimated temperatures should be regarded as only approximate.

Pyrite grain growth is facilitated at high temperatures by the presence of fluids (McClay and Ellis, 1983). Carstens (1986) demonstrated that the presence of an oversaturated fluid on the face of a crystal produces a 'crystalline pressure' that permits the crystal to grow against an imposed force. Although no direct evidence for a fluid on the surface of pyrite during growth exists, the ubiquitous presence of hydrous minerals, such as amphiboles, micas and chlorite in the Deri ores demonstrates the availability of fluids within the sulphide–silicate system during metamorphism (cf. Craig et al., 1991). The presence of a hydrous fluid may therefore be considered to have facilitated porphyroblastic

TABLE 1. Garnet-biotite geothermometry

|  | Garnet1 | Garnet 1 | Garnet 5 | Garnet 5 | Garnet (mean) |
|---|---|---|---|---|---|
| $SiO_2$ | 35.06 | 35.06 | 35.73 | 35.73 | 35.39 |
| $Al_2O_3$ | 20.49 | 20.49 | 20.56 | 20.56 | 20.52 |
| $CaO$ | 2.13 | 2.13 | 2.36 | 2.36 | 2.25 |
| $MnO$ | 13.64 | 13.64 | 13.64 | 13.64 | 13.64 |
| $FeO$ | 26.5 | 26.5 | 25.71 | 25.71 | 26.11 |
| $MgO$ | 0.87 | 0.87 | 0.75 | 0.75 | 0.81 |

|  | Biotite 11 | Biotite 2 | Biotite 4 | Biotite 11 | Biotite (mean) |
|---|---|---|---|---|---|
| $SiO_2$ | 34.69 | 29.2 | 32.69 | 34.69 | 32.29 |
| $CaO$ | 0.13 | 0.35 | 0.14 | 0.13 | 0.21 |
| $MnO$ | 0.37 | 0.39 | 0.41 | 0.37 | 0.39 |
| $FeO$ | 23.96 | 22.91 | 24.09 | 23.96 | 23.65 |
| $MgO$ | 7.61 | 6.14 | 7.14 | 7.61 | 6.96 |
| $TiO_2$ | 1.37 | 1.37 | 1.30 | 1.37 | 1.35 |
| $Na_2O$ | 0.26 | 0.24 | 0.22 | 0.26 | 0.24 |
| $K_2O$ | 8.62 | 7.45 | 8.51 | 8.62 | 8.19 |

Calculated temperature in °C
Ferry and Spear (1978)

|  | 445 | 477 | 455 | 438 | $446 \pm 62$ |
|---|---|---|---|---|---|

Perchuk and Lavrent'eva (1983)

|  | 505 | 525 | 511 | 500 | $505 \pm 39$ |
|---|---|---|---|---|---|

Indares and Martignole (1985)

|  | 566 | 605 | 567 | 547 | $564 \pm 59$ |
|---|---|---|---|---|---|

growth of pyrite in the Deri ores. The timing of porphyroblastic growth is unknown, but the inclusion of $F_2$-folded flaky chlorite (Fig. 6c) in such pyrites suggests that it must be subsequent to $F_2$-folding. Randomly oriented rectangular objects undergoing stress tend to become aligned with their long axes perpendicular to the maximum compressive stress (Hobbs et al., 1976). Pyrite porphyroblasts at Deri are mostly perfect cubes, randomly distributed, and are not aligned along the $S_2$-planes. This is strong evidence in support of post-$F_2/S_2$ growth of coarse pyrite. The lack of any polycrystalline aggregates within these porphyroblasts, confirmed by etching, also indicates that their growth post-dates annealing, and may be ascribed to the retrograde path of regional metamorphism (cf. Craig and Vokes, 1993).

A set of folds defined mainly by softer sulphides and some pyritic streaks along crenulated $S_2$-schistosity (Figs. 5c and 8), with axial traces at characteristically high angles to $S_2$ foliation, may be interpreted to belong to a later $F_3$-generation. This folding is considered tentatively to post-date porphyroblastic pyrite growth but presumably occurred at sufficiently high (450°C) temperatures to allow ductile deformation of pyrite.

Pyrite porphyroblasts also show pulverization (Fig. 7a). These fractures were later filled by ductile sulphides such as galena and chalcopyrite. McClay and Ellis (1983) showed that low metamorphic grade and coarse grain size of pyrite favour brittle deformation, which is consistent with our interpretation that such features of Deri pyrites formed along the retrogressive path of regional metamorphism after growth of porphyroblasts and also following $F_3$-folding.

Smaller pyrite porphyroblasts display coherent fracturing or axial cracking, and are enclosed within an irregular pyritic mass. Interestingly, the irregular pyrite mass surrounding the fractured pyrite grains is totally devoid of any kind of brittle texture suggesting that its growth was later than the enclosed pyrite porphyroblast. This type of

TABLE 2.1. Sphalerite geobarometry

| Sample # | Assemblage | Mole% FeS in Sl | At.% Fe in Po | P (kbar) Hutchinson and Scott (1981) |
|---|---|---|---|---|
| DR6/11 | Sl+Po+Py | 15.8 | 47.8 | 3.8 |
| DR6/11 | Sl+Po+Py | 15.3 | 47.8 | 4.2 |
| DR6/17 | Sl+Po+Py | 16.3 | 47.9 | 3.4 |
| DR6/17 | Sl+Po+Py | 15.7 | 47.9 | 3.9 |

fabric involving two generations of pyrite is best interpreted by the process of fluid assisted mass transfer from the matrix to zones of strain around pyrite porphyroblasts and is widely reported from low-grade metamorphic environments (< 300°C) (cf. McClay and Ellis, 1983). The porphyroblasts, located in high strain zones, yield first by brittle deformation prior to the development of the uneven pyrite envelop. The pyritic mass, on etching, shows local development of some interesting zonal growth patterns (Fig. 6d) which were presumably generated in a diffusion-rate-restricting low-temperature, environment (Yardley, 1989). This feature provides additional evidence for growth of this microfabric in a low-grade metamorphic regime.

The irregular pyrite mass mentioned above locally displays a granoblastic mosaic texture (Fig. 6b), which indicates a further rise of the metamorphic conditions. The replacement of such

TABLE 2.2. Magnetite(Mt) – ilmenite(Ilm) geothermometry

| Sample # | DR6/21 Mt1 | DR6/21 Mt2 | DR6/21 Mt3 | DR6/17 Mt1 |
|---|---|---|---|---|
| $TiO_2$ | 0.46 | 0.46 | 0.46 | 0.45 |
| $Al_2O_3$ | 0.05 | 0.50 | 0.45 | 0.01 |
| FeO | 30.21 | 30.23 | 30.47 | 30.18 |
| $Fe_2O_3$ | 72.46 | 72.44 | 73.03 | 72.40 |
| MnO | 0.05 | 0.05 | 0.03 | 0.02 |
| Usp% | 1.31 | 1.31 | 1.29 | 1.28 |
| LS (1982) | | | | |
| | Ilm1 | Ilm2 | Ilm3 | Ilm1 |
| $TiO_2$ | 50.39 | 50.28 | 50.39 | 50.52 |
| $Al_2O_3$ | 0.03 | 0.01 | 0.03 | 0.01 |
| FeO | 44.94 | 44.83 | 44.97 | 45.06 |
| $Fe_2O_3$ | 6.34 | 6.16 | 6.31 | 6.25 |
| MnO | 0.38 | 0.31 | 0.38 | 0.37 |
| Ilm% | 93.99 | 94.19 | 94.02 | 94.13 |
| LS (1982) | | | | |
| Calculated temperature in °C | | | | |
| SL (1981) | 549 | 547 | 549 | 547 |
| AL (1985) | 555 | 552 | 554 | 551 |

SL = Spencer and Lindsley (1981); LS = Lindsley and Spencer (1982); Anderson and Lindsley (1985)

a pyritic mass by rosette or decussate intergrowths of arsenopyrite is also a common feature. Since such textures can only grow in a stress-free environment, we may relate this arsenopyrite growth to the phase of thermal metamorphism. The granoblastic transformation of the pyritic mass probably indicates peak conditions of this metamorphic episode, which have been estimated from sphalerite geobarometry (3.5 kbar) and magnetite—ilmenite geothermometry (550°C) (Table 2.1 and 2.2) on sulphide-oxide-silicate assemblages displaying hornfelsic textures. The arsenopyrite rosettes also show microfaulting of the individual twined prisms. This leads us to infer that the thermal metamorphic phase was again followed by a mild cataclastic deformation event on the retrogressive path, related to emplacement of the intrusions.

## Conclupionr

The above observations and ensuing discussion bring to light the utility of the study of pyrite microfabrics in the evaluation of the tectono-thermal history of the Deri massive sulphide deposit. The primary growth, deformation, recrystallization and annealing history of the pyrites in the Deri ores are shown schematically in Fig. 10 in terms of the tectono-thermal history of the ore zone rocks, in a manner similar to that presented by Brooker et al. (1987) and Cook et al. (1993) for pyritic deposits at Ducktown and Sulitjelma respectively. This sketch incorporates the initial exhalative hydrothermal conditions (pt. 1) under which the Deri ores formed (Tiwary, 1995) and developed compositional layering, cooling in a sea floor environment (pt. 2), rapid burial and initiation of regional metamorphism in the area. Progressive regional metamorphism during first (pt. 3) and second stages of deformation (pt. 4) produced ductile features in pyrite and reached peak conditions when pyrite was annealed (pt. 5). Along the retrogressive path, pyrite porphyroblasts grew to a coarse size (pt. 6) which was followed by the last phase of open folding (pt. 7) and a phase of
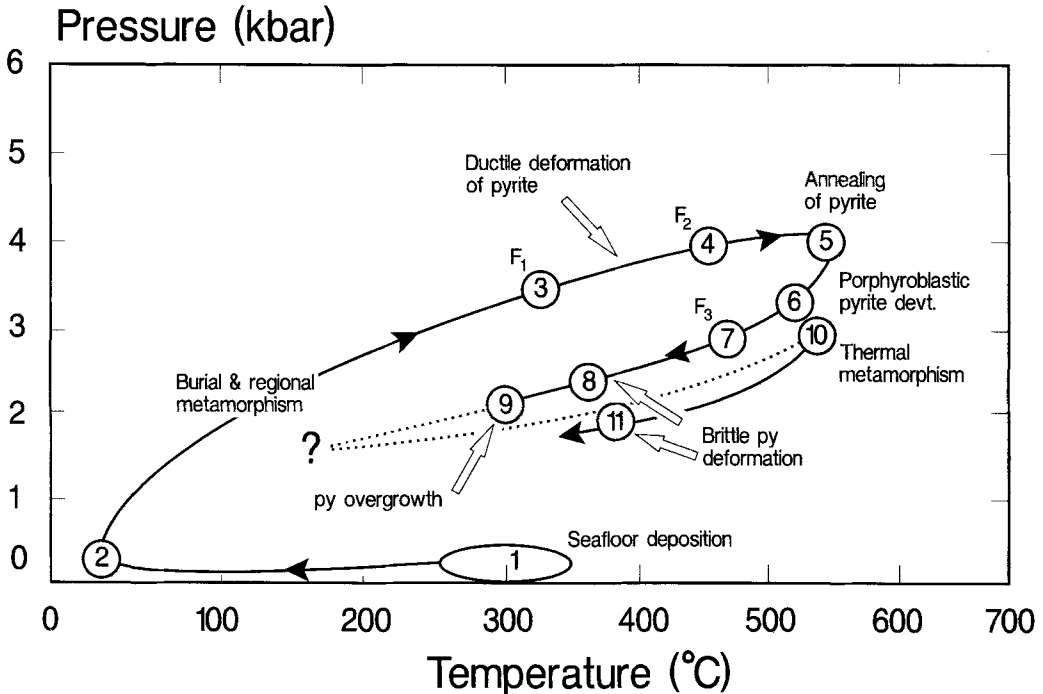


FIG. 10. P—T loop illustrating the successive development of the Deri deposit from syn-diagenetic pyrite formation on the seafloor (pt. 1) and through metamorphism (pts. 2 through 11), in relation to the tectono-thermal events affecting the host rocks of the Deri massive sulphide ores (see text for discussion).

brittle deformation which led to fracturing and axial cracking of the porphyroblasts (pt. 8). Further down the retrogressive path, there was a phase of patchy pyrite growth by pressure solution, enveloping the fractured pyrites (pt. 9). A superimposed thermal metamorphic event resulted in an increase in the geothermal gradient (pt. 10), leading to the annealing of the pyrite envelopes and development of rosette fabric in arsenopyrite. The last signature on the retrogressive path of this metamorphic episode is preserved as microfaults in arsenopyrite twins produced by a penultimate phase of cataclastic deformation (pt. 11).

## References

Anderson, A.T. and Lindsley, D.H. (1985) New (and Final?) model for the Ti magnetite/ilmentite geothermometers and oxygen barometers (abst.). *Trans. Geophysical Union*, **66**, no.18, p.416.

Bhattacharjee, J., Golani, P.R. and Reddy, A.B (1988) Rift related bimodal volcanism and metallogeny in the Delhi fold belt, Rajasthan and Gujarat. *Indian J. Geol.*, **60**(3), 191–9.

Brooker, D.D., Craig, J.R. and Rimstidt, J.D. (1987) Ore metamorphism and pyrite porphyroblast development at the Cherokee mine, Ducktown, Tenessee. *Econ. Geol.*, **82**, 72–86.

Carstens, H. (1986) Displasive growth of authigenic pyrite. *J. Sed. Petrol.*, **56**, 252–7.

Cook, N.J., Halls, C. and Boyle, A.P. (1993) Deformation and metamorphism of massive sulphide at Sulitjelma, Norway. *Mineral. Mag.*, **57**, 67–81.

Cox, S.F., Etheridge, M.A. and Hobbs, B.E. (1981) The experimental ductile deformation of polycrystalline and single crystal pyrite. *Econ. Geol.*, **76**, 2105–18.

Craig, J.R., Vokes, F.M. and Simpson, C. (1991) Rotational fabrics in pyrite from Ducktown, Tenessee. *Econ. Geol.*, **86**, 1737–46.

Craig, J.R. and Vokes, F.M. (1993) The metamorphism of pyrite and pyrite ores. *Mineral. Mag.*, **57**, 3–18.

Deb, M. (1979) Polymetamorphism of ores in Precambrian stratiform massive sulphide deposits at Ambaji-Deri, western India. *Mineral. Deposita*, **14**, 21–31.

Deb, M. (1980) Genesis and metamorphism of two stratiform massive sulfide deposits at Ambaji and Deri in the Precambrian of western India. *Econ. Geol.*, **75**, 572–91.

Deb, M. Thorpe, R.I., Cumming, G.L. and Wagner, P.A. (1989) Age, source and stratigraphic implications of Pb isotope data for conformable, sediment-hosted, base metal deposits in the Proterozoic Aravalli-Delhi orogenic belt, NW India. *Precamb. Res.*, **43**, 1–22.

Deb, M. and Sarkar, S.C. (1990) Proterozoic tectonic evolution and metalligenesis in the Aravalli-Delhi orogenic complex, northwestern India. *Precamb. Res.*, **46**, 115–37.

Deb, M., Thorpe, R.I., Krstic, D., Corfu, F. and Davis, D.W. (in prep.) Zircon U–Pb and Pb isotope evidence for an approximate 1.0 Ga terrane along the western margin of the Aravalli-Delhi orogenic belt, northwestern India.

Ferry, J.M. and Spear, F.S. (1978) Experimental caliberation of the partioning of Fe and Mg between biotite and garnet. *Contrib. Mineral. Petrol.*, **66**, 113–7.

Ghosh, S.K. (1993) *Structural Geology — Fundamentals and Modern Developments.* Pergamon Press, Oxford, 598 pp.

Gopalan, K. (1986) Geochronology of the Precambrian rocks of Rajasthan: problems and prospects. In: *Evolution of the Precambrian crust in the Aravalli mountain belt, Udaipur.* Abst. Pap, 64–5.

Graf, J.L., Bras, J., Fagot, M., Levade, C. and Couderc, J.-J. (1981) Transmission electron microscopic observation of plastic deformation in experimentally deformed pyrite. *Econ. Geol.*, **76**, 738–42.

Graf, J.L. and Skinner, B.J. (1970) Strength and deformation of pyrite and pyrrhotite. *Econ. Geol.*, **65**, 206–15.

Heron, A.M. (1953) The geology of central Rajputana. *Memoir. Geol. Surv. India*, **79**, 389 pp.

Hobbs, B.E., Means, W.D. and Williams, P.F. (1976) *An Outline of Structural Geology.* John Wiley and Sons, New York, 571 pp.

Hutchinson, R.W. and Scott, S.D. (1981) Sphalerite geobarometry in the Cu–Fe–Zn–S system. *Econ. Geol.*, **76**, 143–53.

Indares, A. and Martignole, J. (1985) Biotite–garnet geothermometry in the granulite facies: the influence of Ti and Al in biotite. *Amer. Mineral.*, **73**, 20–47.

Lindsley, D.H. and Spencer, K.J. (1982) Fe-Ti oxide

geothermometry: Reducing analyses of coexisting Ti-magnetite (Mt) and Ilmenite (Ilm) (abst.). *Trans. Amer. Geophys. Union*, **63**, no.18, p. 471.

McClay, K.R. and Ellis, P.G. (1983) Deformation and recrystallization of pyrite. *Mineral. Mag.*, **47**, 527–38.

McClay, K.R. and Ellis, P.G. (1984) Deformation of pyrite. *Econ. Geol.*, **79**, 400–3.

Mookherjee, A. (1971) Deformation of pyrite — A discussion. *Econ. Geol.*, **66**, 200.

Perchuk, L.L. and Lavrent'eva, IV (1983) Experimental investigation of exchange equilibria in the system cordierite–garnet–biotite. In: Saxena, S.K. (ed.) *Kinetics and Equilibrium in Mineral Reactions.* Springer Berlin, Heidleberg, New York, 199–239.

Philipotts, A.R. (1994) *Principles of Igneous and Metamorphic Petrology.* Prentice-Hall of India Pvt. Ltd. , 497 pp.

Roy, A.B. (1988) Stratigraphic and tectonic framework of Aravalli mountain range. *Geol. Soc. India Memoir.*, **7**, 3–31.

Sarkar, S.C. and Deb, M. (1974) Metamorphism of the sulfides of the Singbhum copper belt, India — the evidence from the ore fabric. *Econ. Geol.*, **69**, 1282–93.

Spencer, K.J. and Lindsley, D.H. (1981) A solution model for coexisting iron-titanium oxides. *Amer. Mineral.*, **66**, no.11/12, 1189–201.

Sugden, T. (1987) Kinematic indicators: structures that record the sense of movement in mountain chains. *Geology Today*, May–June, 93–9.

Templemen-Kluit, D.J. (1970) The relationship between sulfide grain size and metamorphic grade of host rocks in some stratabound pyritic ores. *Canad. J. Earth Sci.*, **7**, 1339–45.

Tiwary, A. (1995) *Geological environment, genesis and evolution of the massive sulfide deposit at Deri, Sirohi district, NW India.* Unpubl. Ph.D. thesis, Delhi Univ., 179 pp.

Tiwary, A. and Deb, M. (1997) Geochemistry of alteration zone in bimodal volcanics around Deri massive sulfide deposit, Sirohi district, Rajasthan, India. *J. Geochem. Explor.*, **59**, 99–121 .

Vernon, R.H. (1978) Porphyroblast matrix relationships in deformed metamorphic rocks. *Geologisches Rundschau*, **67**, 288–305.

Vernon, R.H., Peterson, S.R. and Foster, D. (1991) Growth and deformation of porphyroblasts in the Foothill Terrane, Central Sierra Nevada, California: negotiating a microstructural minefield. *J. Metamorph. Geol.*, **11**, 203–22.

Vokes, F.M. (1968) Regional metamorphism of the Palaezoic geosynclinal sulphide ore deposits of Norway. *Trans. Inst. Mining Metall.*, **77**, sect. B, 53–9.

Yardley, B.W.D. (1989) *An Introduction to Metamorphic Petrology.* Longman, London, 248 pp.